Proton stopping power and range calculation using effective atom number and effective electron density from dual energy CT

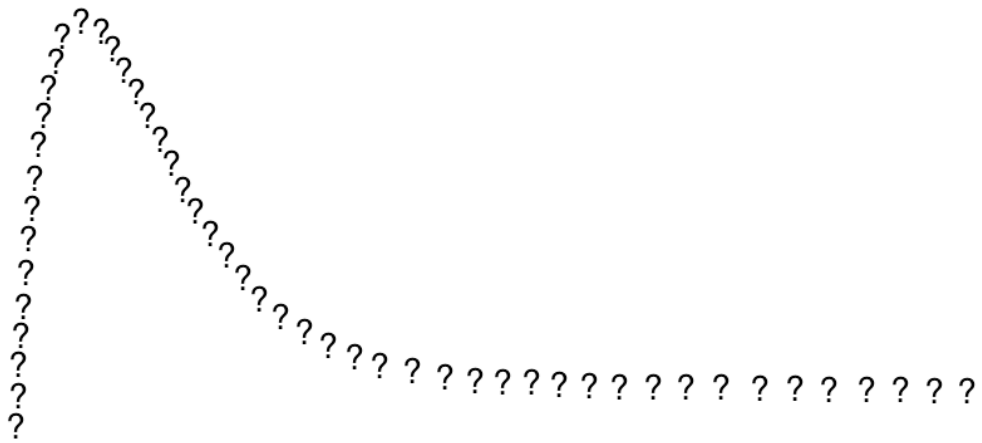

Bachelor thesis applied physics

Bert Bekker

Date: 11-05-2015

Supervisors:
Emiel van der Graaf
Catherine Rigollet

university of groningen

kvi - center for advanced radiation technology

Contents

1. Introduction

Proton therapy is a type of radiation treatment that uses accelerated protons to destroy cancer cells. The advantage of proton therapy in comparison to the conventional radiation therapy with photons, is that the dose of the protons can be more accurately delivered at a certain position. The reason for this is that the dose deposition of a proton sharply peaks at low proton energy after a relatively well-defined penetration depth (figure 1.1). This peak is called the Bragg peak. Beyond the Bragg peak the dose sharply falls to zero. Photons on the other hand have their maximum dose deposition at high photon energies and therefore immediately after penetrating the body. Beyond this peak, the dose deposition decreases very gradually in an exponential manner. This means that the irradiation of healthy tissue around the target tumor is significantly less during proton therapy in comparison to radiotherapy with photons. Consequently, the advantage of proton therapy is that it will result in fewer side effects like secondary tumors, and significantly increases the possibilities to irradiate tumors that are close to radiation sensitive organs. At this moment there are about 50 proton therapy centers worldwide [2]. Most of which have been build in the last few years. In the Netherlands the government has recently appointed 4 locations at which proton therapy centers may be build in the near future. These are: Groningen, Amsterdam, Delft and Maastricht [10]. Groningen and Delft are both starting this year with the construction of a proton therapy center. These are expected to be operating by 2017 [11]. The construction and operation of the proton therapy center at the UMCG in Groningen will be in collaboration with KVI-CART.

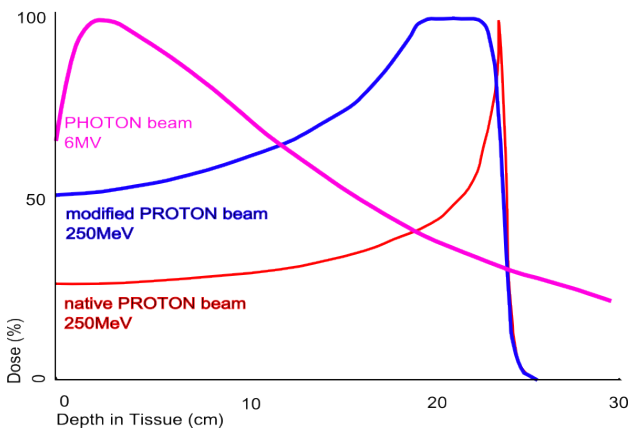

Figure 1.1: *Dose, relative to the maximum dose, plotted against penetration depth for a photon and a proton beam. The sharp peak of the proton beam is the Bragg peak. The blue curve represents a proton beam consisting of protons with different energies so that the peak spreads out* [3].

For the planning of proton therapy treatment it is very important that the stopping power, which is the energy that is lost by the proton per unit of length, in the tissue can be predicted in an accurate way. With the stopping power the dose deposition can be calculated at every point of the trajectory of the proton. The aim of this study is to construct an accurate model that can predict stopping

powers using information from dual energy CT. The dual energy CT information that will be used are the effective atom number and the effective electron density, which have been measured for several materials in a recent study that was also done at KVI-CART [1].

An overview of the method that will be used is illustrated in figure 1.2. Initially two models that can calculate the stopping power from the proton energy will be considered: The Bethe formula, which is a physics based formula [4], and the Bragg Kleeman rule, which is an empirical formula based on scaling laws [5]. The Bethe formula and the Bragg Kleeman rule contain one and two unknowns parameters, respectively. Both models will be fitted to stopping power values for protons in the elements, using the unknown parameters as fitting parameters. The model that gives the best fit will be used for the rest of the procedure. The stopping power values that will be used for fitting can be obtained from either the SRIM dataset from Ziegler [6] or the PSTAR dataset from NIST [7]. These datasets will be compared in this study, and the most appropriate dataset will be used for fitting. Elements with atom number ranging from 1 to 50 will be considered. For every fit, and therefore for every atom number, we then have either one or two fitting parameters, depending on which dataset is chosen. From this, we investigated if a relationship between the fitting parameter(s) and the atom number or electron density can be found.

The fitting parameter(s) of an arbitrary compound can now be found by combining the fitting parameters of all elements that the compound contains using the Bragg additivity rule. The Bragg additivity rule adds the fitting parameters with the electron density that every element in the compound contributes as weighing factor. This will be done for the compounds that were used in the dual energy CT study that measured the effective atom number and the effective electron density [1]. These compounds are mainly tissue-like materials that represent for example bone or lung tissue. The compounds consist of elements with an atom number ranging from 1 to 25 and with effective atom numbers between 6 and 14. The elemental compositions of the compounds used in the study are known so the fitting parameters can be calculated. With this method a relationship between the effective electron density or effective atom number and fitting parameter(s) can be found. This can be used to find the fitting parameter(s), and therefore the stopping power, of a compound with unknown composition (which is often the case in real tissues) when one knows the effective atom number or the effective electron density. This model will be the main result of this study.

From the stopping powers it is also possible to calculate the range of the protons. In a previous experiment at KVI-CART, the proton range has been measured using the same compounds that were used in the dual energy CT study that gave the effective atom number and the effective electron density. In this study the ranges will be calculated from the stopping powers that are obtained from the model. These ranges are then compared to the experimental results.

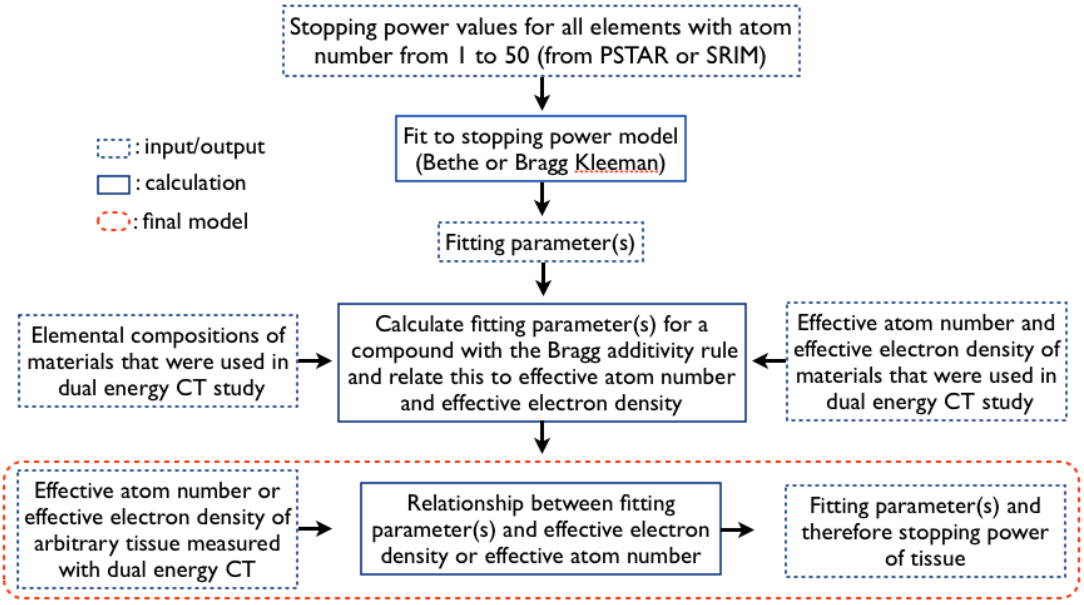

Figure 1.2: *A schematic overview of the approach that will be used to construct the model that calculates stopping powers from effective atom number and effective electron density.*

2. Theory

2.1 Stopping power and the Bragg peak

When a proton travels though a medium it loses energy mainly as a result of Coulomb interactions with electrons. Due to the positive charge of the proton, momentum is transferred to the electrons in the medium. This results in the excitation or ionization of the atoms in the medium. To describe this energy loss of a proton the stopping power is defined. The stopping power is the energy loss per unit of length or -dE/dx of the proton energy.

The Bethe formula

Bethe derived a formula to calculate the stopping power as a function of the proton energy. It is based on the Coulomb interactions of the protons with the electrons. The derivation of the nonrelativistic and semi-classical version of the Bethe formula is quite straightforward. Consider a proton with a velocity *v* that passes an electron in a straight line at a distance *b* as shown in figure 2.1. Since a proton is a relatively heavy particle it is legitimate to assume that it travels in a straight line. The proton and the electron exert a Coulomb force on each other. We assume that the electron is free and at rest. Furthermore, we assume that the interaction takes place sufficiently fast, so that the displacement of the electron during the interaction can be neglected. This means that, due to symmetry around the *y*-axis, the average force over time in the *x*-direction is zero. Therefore only the force in the *y*-direction will be relevant for energy transfer. The momentum that the proton transfers to the electron in the collision then becomes

$$p = \int_{-\infty}^{\infty} F_y \, dt = \int_{-\infty}^{\infty} F \cos\theta \, dt = k_0 \, e^2 \int_{-\infty}^{\infty} \frac{\cos\theta}{r^2} dt = k_0 \, e^2 \int_{-\infty}^{\infty} \frac{b}{r^3} \, dt \tag{2.1}$$

where $k_0 = \dfrac{1}{4\pi \, \varepsilon_0}$ is Coulomb's constant, with ε_0 the permeability of free space. To carry out the integration let *t*=0 represent the time that the proton passes the *Y*-axis. Since the above integral is symmetric around *t*=0 we have

$$p = 2k_0 \, e^2 \int_0^{\infty} \frac{b}{r^3} \, dt = 2k_0 \, e^2 \int_0^{\infty} \frac{b}{(b^2 + (v\,t)^2)^{3/2}} \, dt = 2k_0 \, e^2 \left[\frac{t}{b\sqrt{b^2 + (v\,t)^2}} \right]_0^{\infty}$$

$$= \frac{2k_0 \, e^2}{b \, v} \tag{2.2}$$

The energy transferred in the collision is

$$Q = \frac{p^2}{2m} = \frac{2{k_0}^2 \, e^4}{b^2 \, v^2 \, m} \tag{2.3}$$

where *m* is the electron mass.

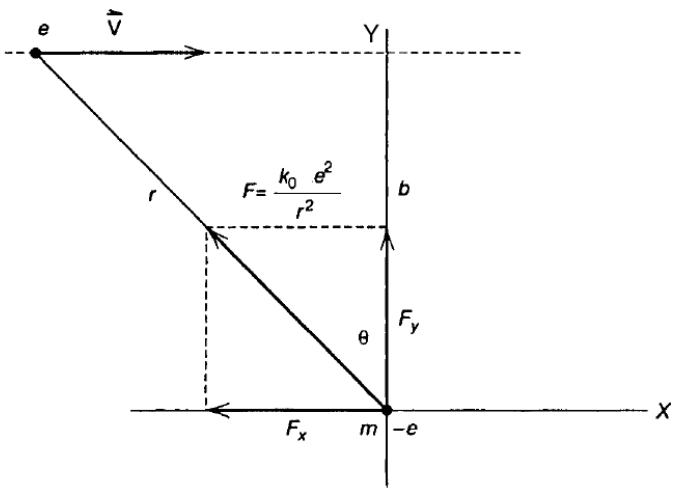

Figure 2.1: *A proton travels along an electron and exerts a force* $\boldsymbol{F}=\boldsymbol{F}_x+\boldsymbol{F}_y$ *on the electron [4].*

When a proton travels through a medium with an electron density of *n* electrons per unit volume, the proton will transfer momentum to all surrounding electrons. From equation 2.3 it follows that the energy that is transferred to an electron depends on the distance *b* between the proton and the electron. This distance is called the impact parameter. The energy transferred to the electrons at a distance ranging from *b* to *b*+*db* when the proton has traveled a distance *dx* is

$$-dE = 2\pi\, b\, db\, dx\, n\, Q(b) \tag{2.4}$$

For an illustration of this infinitesimal volume of electrons, see figure 2.2. The stopping power of a proton in a uniform medium now given by

$$-\frac{dE}{dx} = 2\pi\, n \int_{b_{\min}}^{b_{\max}} Q(b)\, b\, db = \frac{4\pi\, n\, k_0^{\,2}\, e^4}{v^2 m} \int_{b_{\min}}^{b_{\max}} \frac{db}{b}$$

$$= \frac{4\pi\, n\, k_0^{\,2}\, e^4}{v^2\, m} \ln \frac{b_{\max}}{b_{\min}} \tag{2.5}$$

The limits of integration $b_{\min}$ and $b_{\max}$ can be estimated as $h/(mv)$ and v/f respectively, with f the orbital frequency and m the electron mass. For this estimation, quantum mechanical considerations were used which will not be discussed here. The final result is

$$-\frac{dE}{dx} = \frac{4\pi\, n\, k_0^{\,2}\, e^4}{v^2\, m} \ln \frac{m\, v^2}{h\, f} \tag{2.6}$$

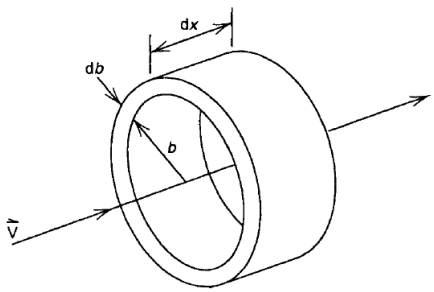

Figure 2.2: *A disk of electron volume with impact parameter between b and db around a proton path of length dx* [4].

Since therapeutic protons have energies up to approximately 250 MeV, they travel at relativistic speeds, and the above nonrelativistic semi-classical formula is not completely valid. But it does give a good insight in the physics behind stopping power. The relativistic quantum mechanical version of the Bethe formula is given by [4]

$$-\frac{dE}{dx} = \frac{4\pi\, n\, k_0^{\,2} e^4}{m\, c^2 \beta^2}\left[\ln\left(\frac{2mc^2\beta^2}{I(1-\beta)}\right) - \beta^2\right] \tag{2.7}$$

Where $\beta = v/c$ is the relativistic speed and I is the mean ionization energy of the medium. When we write $I=2h\cdot f$, it can easily be seen that equation 2.6 and 2.7 are identical at nonrelativistic speeds, that is, if we take $\beta \ll 1$.

From formula 2.7 the origin of the Bragg peak becomes clear. At high velocities and therefore high proton energies, the stopping power is small because of the $1/\beta^2$ term. But as the velocity gets smaller the $1/\beta^2$ term increases rapidly. The logarithmic term on the other hand decreases at low velocities. The combination of these two terms causes a peak in the stopping power.

For the derivation of the Bethe formula several assumptions were made [4] [8]: The protons travel much faster and are much heavier than the target electrons and only Coulomb interactions are relevant. This leads to limitations on the proton energy domain for which the Bethe formula gives accurate results. Besides Coulomb interactions, protons can also lose energy as a result of elastic scattering with atomic nuclei. But only at very low proton energies these interactions make a significant contribution to the proton energy loss and in most cases it can be neglected. Furthermore the protons can capture electrons that reduce the average effective charge op the protons and therefore the stopping power. This effect becomes significant when the proton speed is comparable with the speed of the electrons orbiting around the nuclei, which is at proton energies in the order of 25 keV. To correct for the assumption that the proton velocity is far greater than the orbital velocity of the electrons an extra term needs to be included between the square brackets in equation 2.7. This correction term is called the shell correction term and is relevant for the energies we will be considering (1-250 MeV). The shell correction is at maximum only about 6% of the stopping power. Other correction terms that are often mentioned in literature are the Barkas and the Bloch correction terms that account for the fact that equation 2.7 is only the first Born approximation. These

terms are however not significant for the proton energies we will be considering.

The Bragg additivity rule

The mean ionization energy of a compound, as used in the Bethe formula, can be found with the Bragg additivity rule. This rule combines the excitation energies of all the elements that the compound contains. It can be derived from the fact that every element contributes a certain amount of electrons per unit volume to the compound, which have a certain ionization energy. Therefore every element has a contribution to the stopping power. When all these stopping powers are added we get the total stopping power. From equation 2.7 it then follows that

$$\begin{aligned} -\frac{dE}{dx} &= n_{compound}\, C_1(C_2 - \ln I_{compound}) \\ &= \sum n_{element} C_1(C_2 - \ln I_{element}) \end{aligned} \tag{2.8}$$

where

$$C_1 = \frac{4\pi\, k_0^{\,2}\, e^4}{m\, c^2 \beta^2} \;\; ; \; C_2 = \ln\left(\frac{2m\, c^2 \beta^2}{1-\beta}\right) - \beta^2$$

The summation is over all elements that the compound contains. $n_{element}$ and $n_{compound}$ are the electron densities of the elements and the compound, respectively. When this equation is solved for $I_{compound}$ we obtain the Bragg additivity rule

$$\ln I_{compound} = \sum \frac{n_{element}}{n_{compound}} \ln I_{element} \tag{2.9}$$

The Bragg Kleeman Rule

Another model to calculate the stopping power is the Bragg-Kleeman rule [5] [9]. Unlike the Bethe formula it is an empirical formula. According to the Bragg-Kleeman rule the proton range is given by

$$R = \alpha\, E_i^{\,P} \tag{2.10}$$

where E_i is the initial energy of the proton, α is a material dependent constant and P is a constant that depends on the proton energy. Nevertheless we will use P as material dependant parameter for fitting later in this study. From this equation, an expression for the proton energy after it has travelled a distance x can be derived.

$$R - x = \alpha\, E(x)^P \Leftrightarrow E(x) = \left(\frac{R-x}{\alpha}\right)^{\frac{1}{P}} \tag{2.11}$$

Differentiating the energy with respect to x gives the stopping power

$$-\frac{dE}{dx} = \frac{E^{1-P}}{\alpha P} \tag{2.12}$$

Besides physical constants that are known, the Bethe formula (2.7) and the Bragg Kleeman rule (2.12) have one and two parameters respectively that determine the stopping power for some proton energy. These are the mean ionization energy I for the Bethe formula and α and P for the Bragg Kleeman rule.

2.2 Basics of dual energy CT

Dual energy computed tomography (CT) is a medical imaging technique that uses two different x-ray energies to image a 3-dimensional object. In figure 2.3 the geometry of a dual energy CT scan is shown. Two x-ray tubes with corresponding detectors opposite of the tubes rotate around the scanned tissue. The tubes and detectors are oriented at an angle of 90 degrees with respect to each other and both detectors acquire a dataset of x-ray intensities. By looking at the material specific attenuation at different energies a classification of the composition of the scanned tissues can be made. Therefore dual energy CT is often contemplated as an imaging modality to supply this information for proton therapy planning.

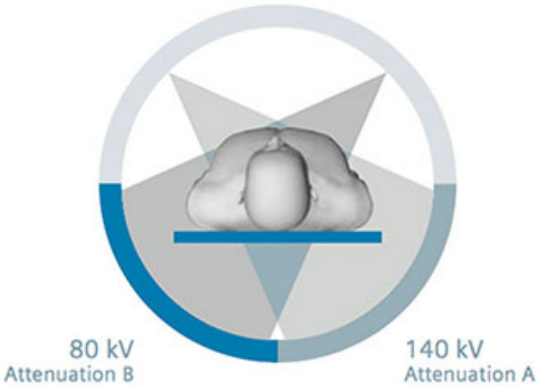

Figure 2.3: *Geometry of a dual energy CT scan. In this figure the two tube potentials are 80 and 140 kV, therefore the maximum x-ray energies from the tubes are 80 and 140 keV respectively [12].*

The attenuation A_j of an incoming x-ray spectrum j in a CT scan is given by

$$A_j = \frac{I_j}{I_{0,j}} = \int_0^\infty w_j(E)\ \exp\left(-\int_L \mu(E,r)dr\right) dE \tag{2.13}$$

where I_j and $I_{0,j}$ are the measured intensities with and without attenuating material respectively [1]. $w_j(E)$ is a factor that accounts for the energy spectrum of the beam and the detector efficiency. $\mu(E,r)$ is the spectral attenuation coefficient, which is integrated over the projection path L. The attenuation coefficient is a measure for the intensity loss of an x-ray beam in a material. As

can be seen from equation 2.13 a large attenuation coefficient means that the intensity loss is large. The spectral attenuation coefficient can also be expressed in the electronic cross section, which is a measure for the attenuation coefficient that is independent of electron density

$$\mu(E,r) = \rho_e \ \sigma(E,Z(r)) \tag{2.14}$$

Here ρ_e is the electron density of the material and $\sigma(E,Z_{eff}(r))$ is the electronic cross section that depends on the energy and the effective atom number Z_{eff}. The ratio of two attenuation coefficients averaged over different energy spectra is given by

$$\frac{\overline{\mu}_1(r)}{\overline{\mu}_2(r)} = \frac{\int_0^\infty w_1(E)\ \sigma(E,Z_{eff}(r))\ dE}{\int_0^\infty w_2(E)\ \sigma(E,Z_{eff}(r))\ dE} \tag{2.15}$$

where $w_1(E)$ and $w_2(E)$ are again factors that accounts for the energy spectrum of the corresponding beam and the detector efficiency. The ratio of the attenuation coefficients can be measured with dual energy CT and $w_1(E)$ and $w_2(E)$ can be determined from measurements with a Compton spectrometer in combination with Monte Carlo simulations [15]. By considering the dependence of the cross section to the energy and effective atom number equation 2.15 can be solved for the effective atom number at each position *r*. Using the effective atom number in combination with the attenuation coefficient (equation 2.14), the effective electron density can then also be determined.

3. Methods

3.1 Stopping power datasets, SRIM vs PSTAR

To obtain a relationship between effective atom number and effective electron density the procedure shown in figure 1.2 will be followed. The first step is to determine which stopping power dataset (PSTAR or SRIM) is the most appropriate for fitting. Proton energies from 1 to 250 MeV will be considered in these fits. To get some insight in which dataset is the most appropriate, the characteristics of the datasets will be considered.

PSTAR

The PSTAR dataset is constructed by the United states National Institute of Standards and Technology (NIST). It consists of mass stopping powers for a large range of proton energies but only for a limited amount of elements. Most elements that are commonly present in human tissues like hydrogen and carbon are included. But for instance magnesium, which may also be present in tissues, is not included in the PSTAR dataset. The total stopping power is calculated from the sum of the stopping power due to Coulomb interactions and the stopping power due to elastic scattering with atomic nuclei [13]. But as mentioned in the theory only the stopping power due to Coulomb interactions, also called electronic stopping power, is significant. At high energies, electronic stopping powers are evaluated using Bethe's stopping power formula. At low energies, fitting formulas are used which are based on experimental stopping power data. The boundary between the high- and low-energy regions is approximately 0.5 MeV. Several correction terms are included in the Bethe formula. These are: the shell correction, the Barkas and Bloch corrections and the density effect correction which is only significant for proton energies above several hundred MeV. The uncertainties of the stopping powers in the high-energy region are stated to be 1% to 2% for elements.

SRIM

The SRIM dataset is constructed by J.F.Ziegler. It contains mass stopping powers for a large range of proton energies and for almost all elements. Just like in the PSTAR dataset the total stopping power is calculated from the sum of the electronic stopping power and the stopping power due to elastic scattering with atomic nuclei. For the electronic stopping power at energies above 1 MeV the Bethe formula is used with comparable correction terms as in PSTAR [8]. In figure 3.1 the significance of the different correction terms used by Ziegler at different energies is shown. The uncertainties of the stopping powers are stated to be about 2%.

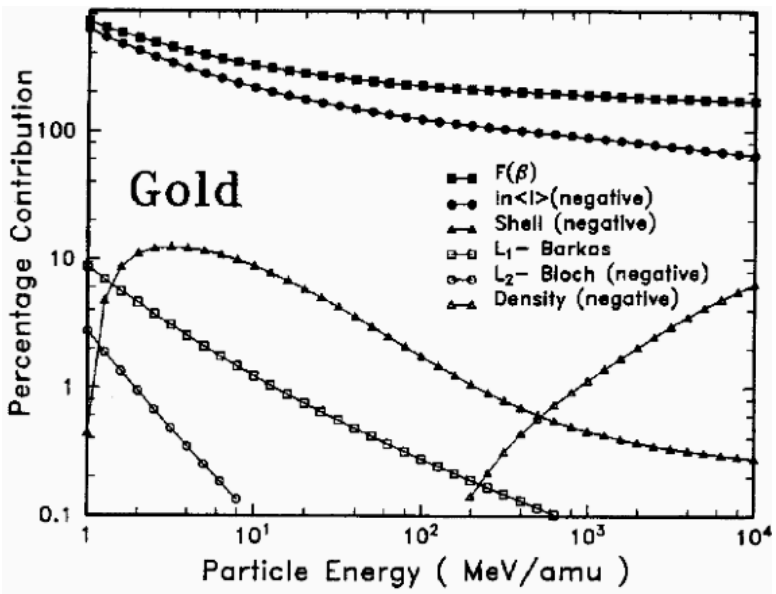

Figure 3.1: *The percentage contribution of the different terms in the Bethe formula plotted against proton energy for gold. F(β) and ln<I> are terms in the basic Bethe formula without correction. The other terms are the correction terms. Taking the sign of the terms into account they add up to 100%. As can be seen from the graph the density correction is not very significant for the energies we will consider [8].*

On first sight the PSTAR and SRIM seem to have an equivalent way of calculating the stopping powers. The accuracy is also comparable. Therefore one would expect that the stopping power values of the two datasets are almost the same. The advantage of SRIM over PSTAR is that it includes all elements.

3.2 Fitting dataset to stopping power formulas

The stopping powers from the dataset for energies from 1 to 250 MeV will be fitted to a stopping power formula as a function of energy. The Bethe formula and Bragg Kleeman rule will be considered, which were discussed in the precious chapter. The stopping power formula that gives the best fit will be used to make fits for all elements with atom number ranging from 1 to 25. To determine which model gives the best fit, the Bethe formula and the Bragg Kleeman rule will be fitted to the stopping power values from the dataset for a number elements. The errors of the two fits will then be compared. All fits are made using a Python script [16] that uses the least square method, minimizing the error between the stopping power values of the dataset and the values of the fitted function. The free parameters used for fitting are α and P in the Bragg Kleeman rule (equation 2.10) and the mean ionization energy I for the Bethe formula (equation 2.7). For every element and therefore every atom number we then have one or two fit parameters depending on whether we choose the Bethe formula or the Bragg Kleeman rule respectively. From this, we can see if a relationship between the fitting parameter(s) and the atom number can be found. From the atom number Z one can easily calculate the electron density

$$\rho_e = N_a \frac{Z}{a_Z} \rho \tag{3.1}$$

where N_a is the Avogadro constant, a_Z is the gram molecular weight of the atoms and ρ is the mass density. Therefore we can also study if there is a relationship between the fitting parameter(s) and the electron density.

For a compound, an effective fitting parameter can be found by combining the fitting parameters of the elements that the compound contains. In the case of the Bethe formula this can be done using the Bragg additivity rule (equation 2.9). The compounds that will be considered are shown in figure 3.2. In a previous study at KVI-CART the effective atom number and effective electron density were calculated for these samples using dual energy CT measurements. The mass fractions of all the elements in the compounds, and the densities of the compounds, are shown in figure 3.2.

ROI No.	Material	Z	1	6	7	8	12	13	14	15	17	20	25	Z'_c	ρ	$\rho_{e,l}/\rho_{e,w}$
		A	1.008	12.011	14.007	15.999	24.305	26.982	28.086	30.974	35.453	40.078	54.938		[gcm^{-3}]	
1	LN-300 lung		8.46	59.37	1.96	18.14	11.19	0	0.78	0	0.10	0	0	7.60	0.29	0.283
2	LN-450 lung		8.47	59.56	1.97	18.11	11.21	0	0.58	0	0.10	0	0	7.57	0.428	0.418
3	AP6 adipose		9.06	72.29	2.25	16.27	0	0	0	0	0.13	0	0	6.19	0.946	0.929
4	BR-12 breast		8.59	70.10	2.33	17.90	0	0	0	0	0.13	0.95	0	6.91	0.981	0.960
5	Water insert		11.19	0	0	88.81	0	0	0	0	0	0	0	7.47	0.998	1.000
6,8,17–21	CT solid water		8.00	67.29	2.39	19.87	0	0	0	0	0.14	2.31	0	7.72	1.014	0.987
7	Solid water M457		8.02	67.22	2.41	19.91	0	0	0	0	0.14	2.31	0	7.72	1.045	1.017
9	Aluminium AlMgSi1		0	0	0	0	1.0	97.2	1.0	0	0	0	0.8	13.25	2.691	2.341
10	BRN-SR2 brain		10.83	72.54	1.69	14.86	0	0	0	0	0.08	0	0	6.07	1.051	1.049
11	LV1 liver		8.06	67.01	2.47	20.01	0	0	0	0	0.14	2.31	0	7.72	1.095	1.066
12	IB3 inner bone		6.67	55.65	1.96	23.52	0	0	0	3.23	0.11	8.86	0	10.39	1.153	1.107
13	B200 bone mineral		6.65	55.51	1.98	23.64	0	0	0	3.24	0.11	8.87	0	10.40	1.159	1.113
14	CB2-30% $CaCO_3$		6.68	53.47	2.12	25.61	0	0	0	0	0.11	12.01	0	10.86	1.330	1.278
15	CB2-50% $CaCO_3$		4.77	41.62	1.52	31.99	0	0	0	0	0.08	20.02	0	12.49	1.560	1.473
16	SB3 cortical bone		3.41	31.41	1.84	36.50	0	0	0	0	0.04	26.81	0	13.59	1.823	1.699

Figure 3.2: *Elemental compositions (weight percentages) of tissue like compounds. ρ is the density of the compounds [1].*

To calculate the mean ionization energy fitting parameter using the Bragg additivity rule we need to know the electron density fractions instead of the mass fractions of the elements in the compounds. The electron density that an element contributes is given by

$$\rho_e^Z = N_a \frac{Z}{a_Z} \rho_{compound} \, C_Z \tag{3.2}$$

with a_Z the gram molecular weight of element Z, $\rho_{compound}$ the mass density of the compound that is given in the table and C_Z the mass fraction of element Z in the compound. For the total electron density of the compound we sum over all the atom numbers in the compound

$$\rho_e^{compound} = N_a \, \rho_{compound} \sum_Z \frac{Z}{a_Z} \, C_Z \tag{3.3}$$

With these formulas in combination with the Bragg additivity rule we can find the combined mean ionization energy fitting parameter for the compounds in the table in figure 3.2. The calculations for this will be done using a Python script. Since the effective electron densities and the effective atom numbers of these compounds are known, plots can be made that shows the relationship between the mean ionization energies of the compounds and the effective atom numbers and the effective electron densities. The desired result would be that

the points in the graphs will form a smooth curve so that there is a clear relationship between the ionization energy fitting parameter and the effective atom number or effective electron density. This would mean that one can find a value for the ionization energy fitting parameter to some accuracy for a tissue when the effective electron density or the effective atom number is known. This ionization energy fitting parameter can be plugged into the Bethe formula again to obtain the stopping power. In the Bethe formula the electron density is also a variable that needs to be known. In this study the effective electron density is used since the effective electron density is almost equivalent to the real electron density [1].

3.3 Range calculation

The ranges of protons traveling trough a medium can be calculated with the inverse of the stopping power. The range is given by

$$R = \int_0^{E_0} \frac{dx}{dE} dE \tag{3.4}$$

where the integration is over the proton energy from E_0, which is the energy at which the proton enters the medium, to the point where the proton has lost all of its energy.

In an experiment at KVI-CART, ranges were measured of protons in some of the compounds listed in figure 3.2. The setup of this experiment is shown in figure 3.3. Accelerated protons enter a slice of material that is a few centimeters thick. The material is surrounded by water, so after the protons have traveled through the material the resuming trajectory is in water. At a certain distance the energy deposition peaks (Bragg peak) and then drops rapidly to zero. The range is defined here as the distance at which the energy deposition is 80% of its maximum value [14]. By taking the difference between the range in water and the range in the slice of material in combination with water the range difference ΔR, as shown in the figure can be calculated.

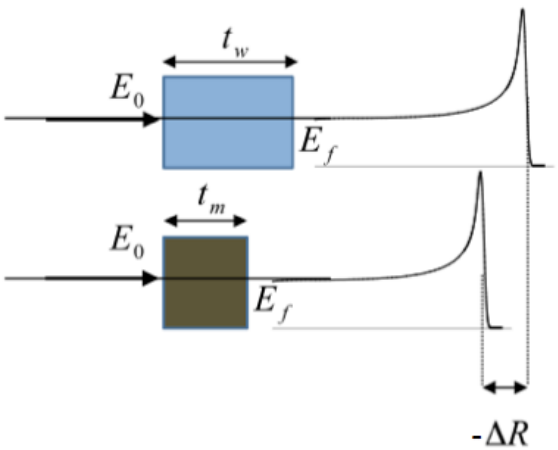

Figure 3.3: *The setup of the range experiment. t_m is the thickness of the slice of material and t_w is the thickness of a water sample that would yield the same proton energy loss, also called the water equivalent thickness of t_m. E_0 is the energy at which the proton enters the material and E_f is the energy at which the proton leaves the material.*

ΔR can be calculated from the stopping power using the formula

$$\Delta R = t_m - \int_{E_f}^{E_0} \left(\frac{dx}{dE} \right)_{water} dE \tag{3.5}$$

where $\left(\frac{dx}{dE} \right)_{water}$ is the inverse stopping power of water. The other symbols are explained in the description of figure 3.3. The material thickness t_m can be expressed in the inverse stopping power of the material.

$$t_m = \int_{E_f}^{E_0} \left(\frac{dx}{dE} \right)_{material} dE \tag{3.6}$$

The energy E_0 at which the proton enters the sample is unknown. But it can be calculated when the following equation is solved for E_0

$$R_{water} = \int_{0}^{E_0} \left(\frac{dx}{dE} \right)_{water} dE \tag{3.7}$$

where R_{water} is the range of the protons in water, which was obtained from the range experiment. The inverse stopping power can be calculated from the stopping power model. The thicknesses of the samples are known and therefore equation 3.6 can be solved for E_f. This equation will be solved using a Python script. The resulting E_f can then be plugged into equation 3.5. In combination with the stopping power in water that can also be calculated with the model and the thicknesses of the material samples ΔR can be obtained. The calculated values for ΔR will be compared with the measured values for ΔR.

4. Results

4.1 SRIM and PSTAR compared

In figure 4.1 a plot of the ratio of the mass stopping powers from SRIM and PSTAR for hydrogen is shown. When the ratio is 1 the stopping powers are the same. The deviation from 1 is at maximum 0.006 or 0.6%. This plot has been made for oxygen and copper as well, and all plots showed that the difference between the stopping powers from PSTAR and SRIM is within 1%. Therefore we conclude that the SRIM and the PSTAR stopping powers are almost equivalent. This means that the SRIM dataset will be used for the rest of the process because SRIM gives stopping power values for more elements than PSTAR.

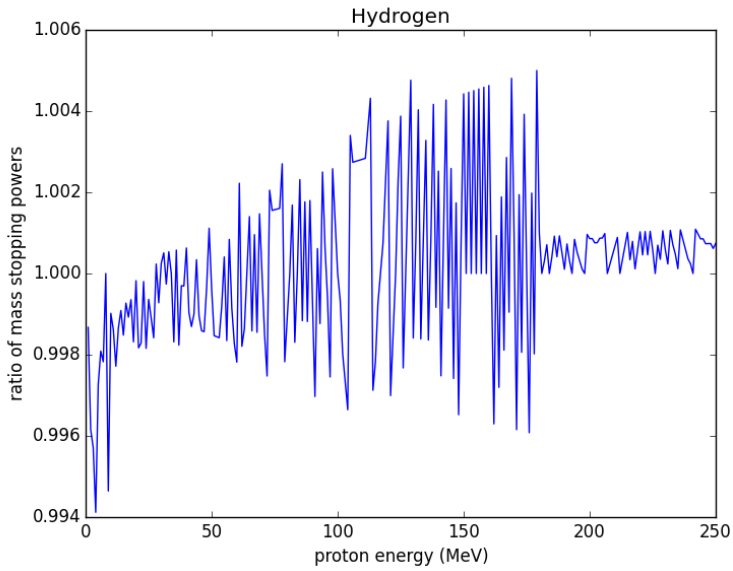

Figure 4.1: *The ratio of the mass stopping powers from PSTAR and SRIM plotted against proton energy.*

4.2 Bethe and Bragg Kleeman compared

In figure 4.2 the blue line represents the ratio of the stopping power values from the Bethe formula fitted to the SRIM stopping power values and the SRIM stopping power values. The red line represents the ratio of the stopping power values from the Bragg Kleeman rule fitted to the SRIM stopping power values and the SRIM stopping power values. The stopping power formula that corresponds to the graph that stays closest to 1 will be the one that gives the best fit. Which is without any doubt the Bethe formula. The stopping powers in this graph are for calcium. But also stopping powers for zinc, lithium, helium and hydrogen were considered. All graphs showed that the Bethe formula gives a significantly better fit. The maximum error was for all graphs in the low energy region and was at maximum 5%. This makes sense because the correction terms, which are not used in the fit formula, make the most significant contribution to the stopping power in the low energy region as was shown in figure 3.1. Another advantage of the Bethe formula is that it only has one fitting parameter. Which makes it much easier to calculate the effective fitting parameter of a compound. This can be done with the Bragg additivity rule. Therefore the Bethe formula will be used in the rest of this thesis.

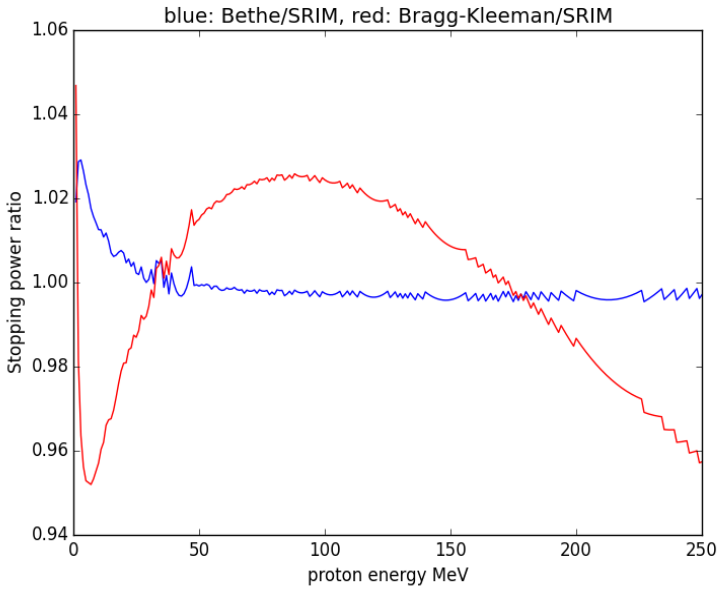

Figure 4.2: *Blue: the ratio of the stopping powers calculated from the the Bethe fit and the stopping powers from SRIM. Red: the ratio of the stopping powers calculated from the the Bragg Kleeman fit and the stopping powers from SRIM.*

4.3 Relation between ionization energy and effective atom number

For every element with atom number up to 25 the Bethe formula is fitted to the stopping powers from SRIM in the energy range from 1 to 250 MeV. The result is the relationship between mean ionization energy fitting parameter and atom number represented in figure 4.3 by the blue dots. Every element is one dot. As can be seen from the graph there is quite a clear relationship between the mean ionization energy fitting parameter and the atom number. This is logical because a larger atom number means a higher potential and therefore a positive relationship between atom number and mean ionization energy makes sense. In the same figure the relationship between the mean ionization energy of the compounds and the effective atom number is shown. The mean ionization energies of the compounds are calculated using the Bragg additivity rule, which combines the mean ionization energy fitting parameters of the elements. Note that the horizontal axis is used for two different scales. For the element the values on the axis represents atom numbers, and for compounds the axis represents effective atom numbers. These are closely related but not the same. Some of the compounds are labeled in the graph. These are some of the compounds that will be used for range calculation. Except for aluminum the graph of the compounds is quite smooth.

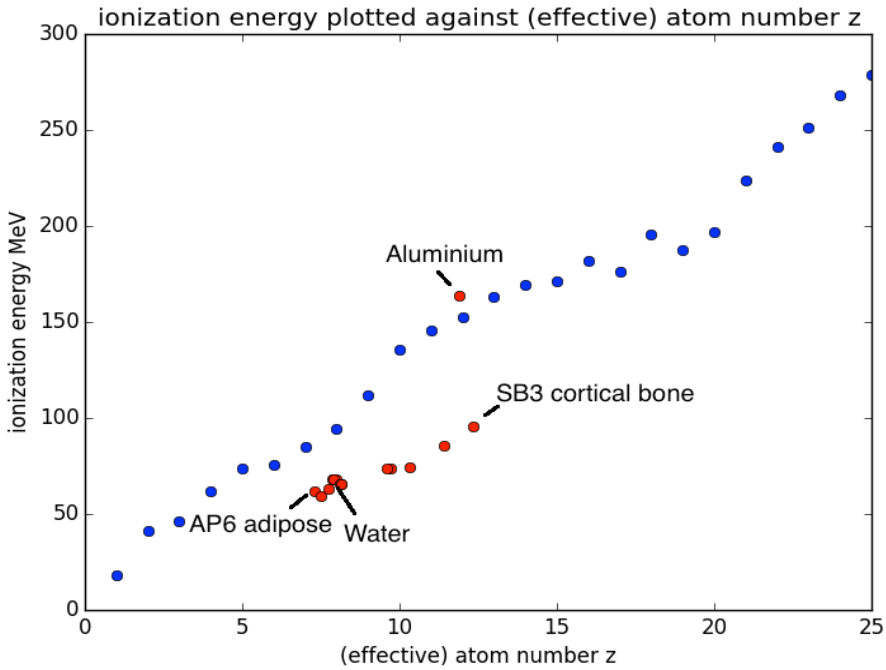

Figure 4.3: *The mean ionization energy plotted against atom number for elements (blue) and plotted against effective atom number for compounds (red).*

In order to find a relationship between effective atom number and mean ionization energy the curve of the compounds as shown in figure 4.3 has been interpolated and extrapolated with a fit function. For this purpose a third order polynomial was used. The fit is shown in figure 4.4. Aluminum was left out because it disturbs the result too much and because aluminum is not very relevant for medical purposes anyway.

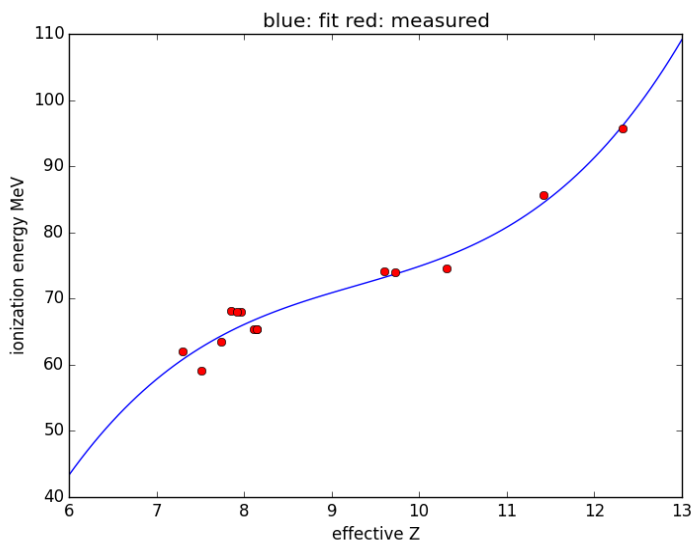

Figure 4.4: *A fit function was used to find a relationship between mean ionization energy and effective atom number Z.*

4.4 The relation between ionization energy and effective electron density

For every atom number the electron density can be calculated with equation 3.1. With the relationship between mean ionization energy and atom number for elements one can therefore easily obtain a graph of the mean ionization energy as a function of electron density for elements. This plot is represented by the blue dots shown in figure 4.5. There seems to be no relationship between the mean ionization energy and electron density whatsoever. This is not surprising because the mean ionization energy is considered to be independent of the density, while the electron density is very closely related to the ionization energy. Nevertheless there is some relationship between the mean ionization energy of the compounds calculated with the Brag additivity rule and the effective electron density represented by the red dots in figure 4.5. Apparently there is some relationship between the elemental composition of tissue-like samples and the electron density.

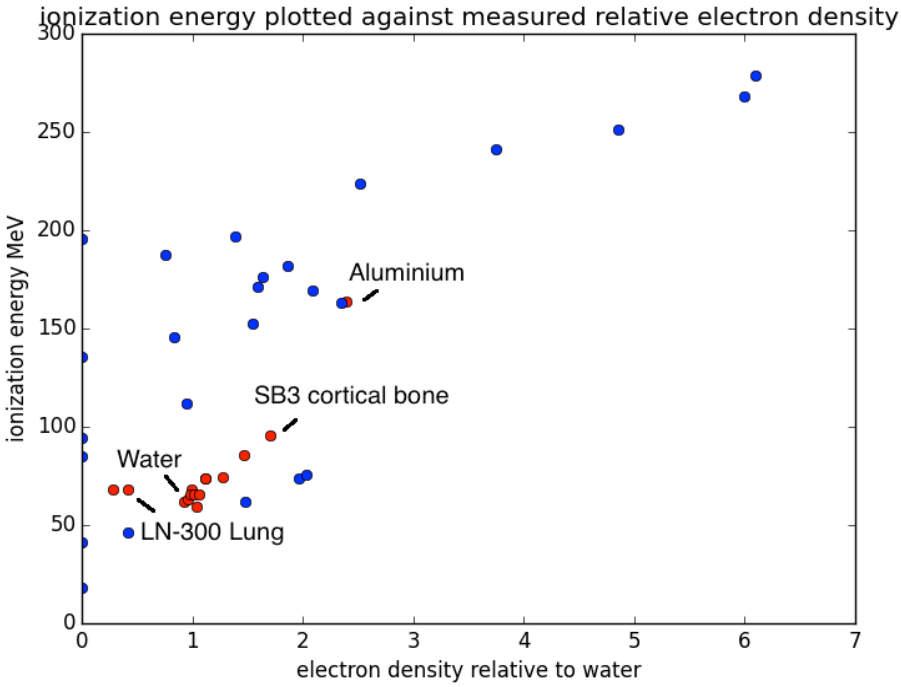

Figure 4.5: *The mean ionization energy plotted against electron density for elements (blue) and plotted against effective electron density for compounds (red) since effective electron density and regular electron density are almost equivalent the axis can be considered as representing only the regular electron density. All electron densities divided by the electron density of water.*

To find a function for the relationship between the mean ionization energy and effective electron density the red points in figure 4.5 are again interpolated and extrapolated using a fit function. This is shown in figure 4.6. Two linear functions on different domains are used as fit function.

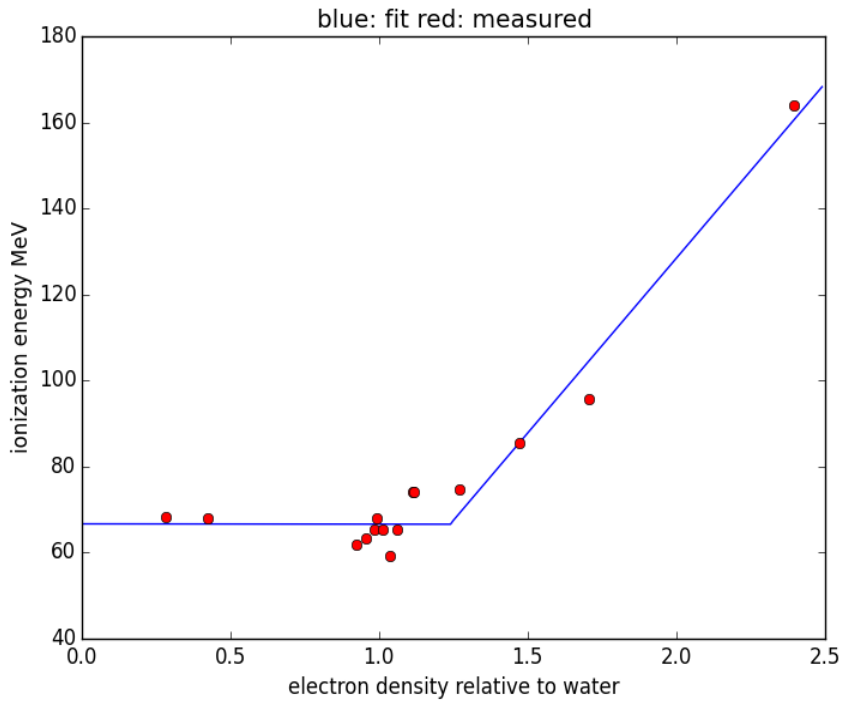

Figure 4.6: *A fit function was used to find a relationship between mean ionization energy and effective electron density.*

4.5 proton ranges

In figure 4.7 the ΔR values for several materials calculated with the method described in section 3.3 are shown. The column with the title 'Electron density model' represents the ΔR values that were calculated using stopping powers that were calculated with the relationship between mean ionization energy and effective electron density. The column with the title 'Z-effective model' represents the ΔR values that were calculated using stopping powers that were calculated with the relationship between mean ionization energy and effective atom number. The energy at which the proton enters the material E_0 was calculated using equation 3.7. For the stopping power of water calculated with the z-effective model as well as the stopping power calculated with the electron density model equation 3.7 was solved. The two outcomes only differed 0.2 electron volts and the average value (184.25 MeV) was taken for the range calculation. The experimental values are the values that were measured in the experiment at KVI-CART. The errors in the table are the deviations of the calculated ΔR from the experimental values. Except for aluminum in the Z-effective model, the errors are within a millimeter.

	Elec. dens. model		Z-effective model		experimental
Material	ΔR (mm)	error	ΔR (mm)	error	ΔR (mm)
water	0.225	0.225	-0.212	0.212	0
Solid Water	0.545	0.750	0.108	0.097	-0.205
AP6 adipose	1.943	0.776	1.325	0.158	1.167
SB3 cort bone	-7.725	0.084	-8.342	0.533	-7.809
Aluminium	-10.042	0.352	-11.911	2.221	-9.690
LN450 lung	27.379	0.177	26.952	0.250	27.202
BR12 Breast	1.172	0.208	0.690	0.274	0.964
LV1 Liver	-0.995	0.199	-1.384	0.190	-1.194

Figure 4.7: *Calculated and experimental ΔR values for several materials. All values are in millimeters.*

5. Conclusion

The main goal of this study was to construct a model that can accurately calculate stopping power values from effective electron density and effective atom number from dual energy CT. After considering both the Bragg Kleeman rule and the Bethe formula we concluded that the Bethe formula is the most appropriate basis for such a model. The Bethe formula gave the best fit to the SRIM stopping power values and has only one free fitting parameter which makes it easy to work with. For fitting the SRIM stopping power values were used. Comparing the physical basis and the stopping power values of the PSTAR and the SRIM dataset showed that there is not much difference between the two. But because SRIM includes more elements this dataset was used.

The mean ionization energy plotted against effective atom number for compounds resulted in a smooth curve. As mentioned in section 4.3 there is a logical physical basis for this relationship. Only aluminum gave an inconsistent result and was not included in the final fit. Aluminum was the only non tissue like sample that was considered and therefore is less significant for medical purposes. The reason for this large deviation of aluminum is not known but may be related to the way the effective atom numbers are calculated from dual energy CT data. The mean ionization energy plotted against effective electron density also gave a curve that was also more or less smooth. The physical basis of such a relationship in general is not present. But in the case of tissues there may be some relationship between the elemental composition of tissue like samples and the electron density. In the final fit of the relationship between mean ionization energy and effective electron density aluminum was included.

The range calculations can be seen as a validation for the stopping power models since stopping powers calculated from the models were used to calculate the ranges. The range differences shown in figure 4.7 deviate in most cases less than 1 mm from the experimental values. The range calculations gave a mean error of 0.35 mm for the electron density model and 0.49 mm for the Z-effective model (without aluminum 0.25 mm). For proton therapy an accuracy of 1 to 2 millimeter is required so these results are encouraging. One should however note that the samples considered were only a few centimeters thick. This means that the mean error for the ranges on the decimeter scale, which is the case for proton therapy, will be about a factor ten larger. Therefore this model still needs some refinement. To make this model more reliable more tissue like samples should be included in the model. Another method of calculating the effective atom number can also possibly improve the result. The validation of this model is now based on a limited number of tissues. To increase the accuracy of the validation of the model, more samples with measured ranges should be considered.

6. Bibliography

[1] J.K. van Abbema, M. van Goethem, M.J.W. Greuter, A van der Schaaf, S. Brandenburg, E.R. van der Graaf 2015, Relative electron density determination using a physics based parametrization of photon interactions in medical DECT

[2] http://www.ptcog.ch/index.php/facilities-in-operation, march 2015

[3] http://en.wikipedia.org/wiki/Bragg_peak, March 2015

[4] J.E.Turner 2007, Atoms radiation and radiation protection 3rd edition, ISBN 9783527406067

[5] B.W. Kleeman, R.D.Kleeman 1905, on the alpha particles of radium and their loss of range in passing through various atoms and molecules

[6] http://www.srim.org/#SRIM, March 2015

[7] http://physics.nist.gov/PhysRefData/Star/Text/PSTAR.html, March 2015

[8] J.F.Ziegler 1999, The stopping of energetic light ions in elemental matter

[9] R.Zhang, W.D.Newhauser 2009, Calculation of water equivalent thickness of materials of arbitrary density, elemental composition and thickness in proton beam irradiation

[10] http://www.umcgroningenptc.nl/protonen-in-nederland, April 2015

[11] http://fd.nl/economie-politiek/1094490/groningen-en-delft-zetten-miljoeneninvestering-in-protonenklinieken-door, April 2015

[12] http://www.dsct.com/index.php/dsct-basics/introduction/dual-source-ct-imaging/, April 2015

[13] http://physics.nist.gov/PhysRefData/Star/Text/programs.html, April 2015

[14] H.Paganetti 2012, proton therapy physics, ISBN 978-1-4398-3645-3

[15] H. A. Duisterwinkel, J. K. van Abbema, M. J. van Goethem, R. Kawachimaru, L. Paganini, E. R. van der Graaf, S. Brandenburg 2015, Spectra of clinical CT scanners using a portable Compton spectrometer

[16] https://www.python.org/, May 2015